J. Coat. Technol. Res., **14** (1) 195–205, 2017
DOI 10.1007/s11998-016-9842-0

Surface-initiated growth of copper using isonicotinic acid-functionalized aluminum oxide surfaces

Cathren E. Gowenlock, Virginia Gomez, James D. McGettrick, Enrico Andreoli, Andrew R. Barron

Abstract Isonicotinate self-assembled monolayers (SAM) were prepared on alumina surfaces (A) using isonicotinic acid (*i*NA). These functionalized layers (*i*NA-A) were used for the seeded growth of copper films (Cu-*i*NA-A) by hydrazine hydrate-initiated electroless deposition. The films were characterized by scanning electron microscopy (SEM), electron-dispersive X-ray spectroscopy, atomic force microscopy, X-ray photoelectron spectroscopy, X-ray diffraction, and advancing contact angle measurements. The films are Cu^0 but with surface oxidation, and show a faceted morphology, which is more textured (R_q = 460 ± 90 nm) compared to the SAM (R_q = 2.8 ± 0.5 nm). In contrast, growth of copper films by $SnCl_2/PdCl_2$ catalyzed electroless deposition, using formaldehyde (CH_2O) as the reducing agent, shows a nodular morphology on top of a relatively smooth surface. No copper films are observed in the absence of the isonicotinate SAM. The binding of Cu^{2+} to the *i*NA is proposed to facilitate reduction to Cu^0 and create the seed for subsequent growth. The films show good adhesion to the functionalized surface.

C. E. Gowenlock, V. Gomez, E. Andreoli, A. R. Barron (✉)
Energy Safety Research Institute (ESRI), College of Engineering, Swansea University, Bay Campus, Swansea, Wales SA1 8EN, UK
e-mail: a.r.barron@swansea.ac.uk; arb@rice.edu

J. D. McGettrick
SPECIFIC, Baglan Bay Innovation & Knowledge Centre, College of Engineering, Swansea University, Baglan, Port Talbot, Wales SA12 7AX, UK

A. R. Barron
Department of Chemistry and Department of Materials Science and Nanoengineering, Rice University, Houston, TX 77005, USA

Keywords Copper, Isonicotinic acid, Aluminum oxide, Thin film, Electroless deposition

Introduction

As a thin film deposition method, electroless deposition (ELD) is relatively simple and less expensive, is performed at ambient or low temperature, and can be potentially selective.[1,2] In comparison with electrochemical deposition, ELD occurs via chemically promoted reduction of metal ions without external current and is thus suitable for a wide range of substrates, including insulators. ELD has also found application in the coating of a range of nanoparticles.[3,4] It is used in a wide range of applications to deposit copper including the preparation of chip interconnects.[5,6]

Self-assembled monolayers (SAMs) with varying functionalities have been demonstrated to direct the assembly of inorganic thin films via ELD.[7–9] The reason for this selective deposition is that the functionality of the SAM acts as an accelerator molecule to control crystal heterogeneous nucleation and growth. Amino groups, catechols, and thiols have all been used to seed metallic ELD copper growth on surfaces,[10–12] and they can also be used to assist in electrochemical deposition.[13] Pyridine and related derivatives represent one of the most common ligand types for copper,[14–17] and we have used this in our work with copper-specific complexes.[18–21] We have recently reported that isonicotinic acid (Fig. 1) functionalization of alumina nanoparticles allows for the highly stable binding of copper acetate ($Cu_2(O_2CMe)_4$),[22] and we have also shown that its derivatives allow for binding of metals to specific locations on nanoparticles.[23] The use of the acid form allows for the covalent binding to the aluminum oxide surface,[24–27] and thus we have investigated the ability of isonicotinic acid-functionalized alumina thin films to promote the ELD of copper with

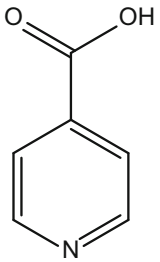

Fig. 1: Structure of isonicotinic acid

hydrazine as a reducing agent. In order to show the robustness of the method, formaldehyde with tin/palladium catalysis was used as an alternative reducing agent. These results are presented herein.

Experimental

Materials and methods

Isonicotinic acid (*i*NA), copper(II) sulfate pentahydrate ($CuSO_4.5H_2O$), hydrazine hydrate ($N_2H_4.H_2O$), ethylenediaminetetraacetic acid (EDTA), formaldehyde solution (37 wt%), tin(II) chloride ($SnCl_2$), and palladium(II) chloride ($PdCl_2$) were purchased from Sigma-Aldrich, Ltd. and used as received. Alumina-coated silicon wafers prepared by atomic layer deposition (ALD) were provided by Natcore Technology, Inc. (NTX.V).

The morphologies of the samples and their elemental composition were examined using scanning electron microscopy (SEM) and quantitative electron-dispersive X-ray (EDX) spectroscopy with a Hitachi Field Emission S-4800 SEM with an Inca electron-dispersive X-ray detector (Oxford Instruments, Abingdon, UK) for EDX experiments. The surfaces of the samples were studied by a JPK NanoWizard II Atomic Force Microscope (AFM) using noncontact cantilevers (RTESP, Bruker). Intermittent contact mode was used to take 20 × 20 μm images for each sample at a scan rate of 0.5–1 Hz and an image resolution of 512 × 512 pixels. The images were analyzed using JPK offline processing software. The mean roughness root-mean-square (R_q), averaged roughness (R_a), and the peak-to-valley roughness (R_t) were determined from the AFM scans for each sample.

X-ray photoelectron spectra (XPS) were recorded on a Kratos Axis Supra instrument (Kratos Analytical, Manchester, UK) using a monochromated Al-K_α source. All spectra were recorded using a charge neutralizer to limit differential charging and subsequently calibrated to the main adventitious C_xH_y carbon peak at a binding energy of 284.8 eV. Survey scans were recorded at a pass energy of 160 eV and high-resolution data at a pass energy of 20 eV. Data were fitted using CASA XPS with Shirley backgrounds. X-ray diffraction (XRD) patterns were recorded on a Brüker D8 DISCOVER diffractometer in Bragg–Brentano geometry with a Cu-K_α X-ray source (λ = 0.15418 nm) and analyzed using Match 2 software.

Advancing water contact angle measurements were made under ambient conditions using the sessile drop shape method. Contact angles were calculated using Drop Shape Analysis DSA1 software provided with the Kruss FM40 Easydrop goniometer (Kruss, Germany). Contact angles on three different regions of each sample were measured and averaged.

Preparation of isonicotinic acid-functionalized alumina thin films

Isonicotinic acid-functionalized alumina surfaces were prepared following a modification of the literature protocols.[27,28] The alumina-coated silicon wafer (100) substrates were immersed in an aqueous solution of isonicotinic acid (0.2 M) and left for 6 days at 50°C. Wafers were removed and rinsed sequentially with water (5 × 30 mL), acetone (1 × 30 mL), and benzene (1 × 30 mL) to ensure the removal of any unreacted isonicotinic acid and then oven dried overnight at 80°C.

Copper ELD using hydrazine as the reducing agent

Copper plating of alumina wafers by electroless deposition was carried out following an adaptation of a literature protocol.[11] An aqueous room-temperature solution (40 mL) of $CuSO_4{\cdot}5H_2O$ (0.054 M) acted as a source of copper(II) ions, stabilized by chelation with EDTA (0.034 M). Coupons (20 mm^2) of pristine (unfunctionalized) alumina-coated silicon wafer (A) and isonicotinic acid-functionalized alumina wafer (*i*NA-A) were added to the solution prior to the addition of hydrazine hydrate solution (1.3 mL), which triggers the electroless deposition process. After completion of electroplating, the wafer pieces were removed from the solution, washed copiously with deionized water (5 × 30 mL) and ethanol (5 × 30 mL), and then oven dried overnight at 80°C.

Copper ELD using formaldehyde as the reducing agent

Alumina wafers were also copper plated by an alternative electroless deposition process, using a traditional tin- and palladium-based activation process and formaldehyde solution.[29] A filter paper (5 cm in diameter) was immersed in a sensitizer solution (50 mL) of $SnCl_2$ (0.04 M) and HCl (0.5 M) for 1 min, rinsed with deionized water, and then immersed in an activator solution (50 mL) of $PdCl_2$ (1 mM) and HCl (0.05 M) for 1 min. The filter paper was then rinsed with deionized water. An aqueous solution

(100 mL) of $CuSO_4{\cdot}5H_2O$ (0.04 M) and EDTA (0.04 M) at 70°C was adjusted to pH 12 with NaOH, and coupons (20 mm^2) of pristine (unfunctionalized) alumina-coated silicon wafer (A) and isonicotinic acid-functionalized alumina wafer (*i*NA-A) were added to the solution. Formaldehyde solution (0.08 M) was added, followed by the palladium-treated filter paper. After completion of electroplating, the wafer pieces were removed from the solution, washed copiously with deionized water (5 × 30 mL) and ethanol (5 × 30 mL), and then oven dried overnight at 80°C.

Results and discussion

Figure 2 shows a schematic diagram of the functionalization of alumina-coated Si wafer with isonicotinic acid (*i*NA) and the subsequent Cu ELD reaction. In order to determine the effects of the *i*NA, unfunctionalized wafers were also exposed to the ELD solutions. Two ELD reactions were investigated using hydrazine (equation 1) or formaldehyde (equation 2) as the reducing agent.[11,29] The latter reaction uses a tin- and palladium-based activation process.

$$CuSO_4 \cdot 5H_2O + N_2H_4 \rightarrow Cu + N_2 + H_2SO_4 + 5H_2O \quad (1)$$

$$Cu^{2+} + 2H_2CO + 4OH^- \rightarrow 2HCO_2^- + 2H_2O + H_2 \quad (2)$$

Morphology

The surface morphology of the alumina-coated wafers was examined using SEM prior to and after function-

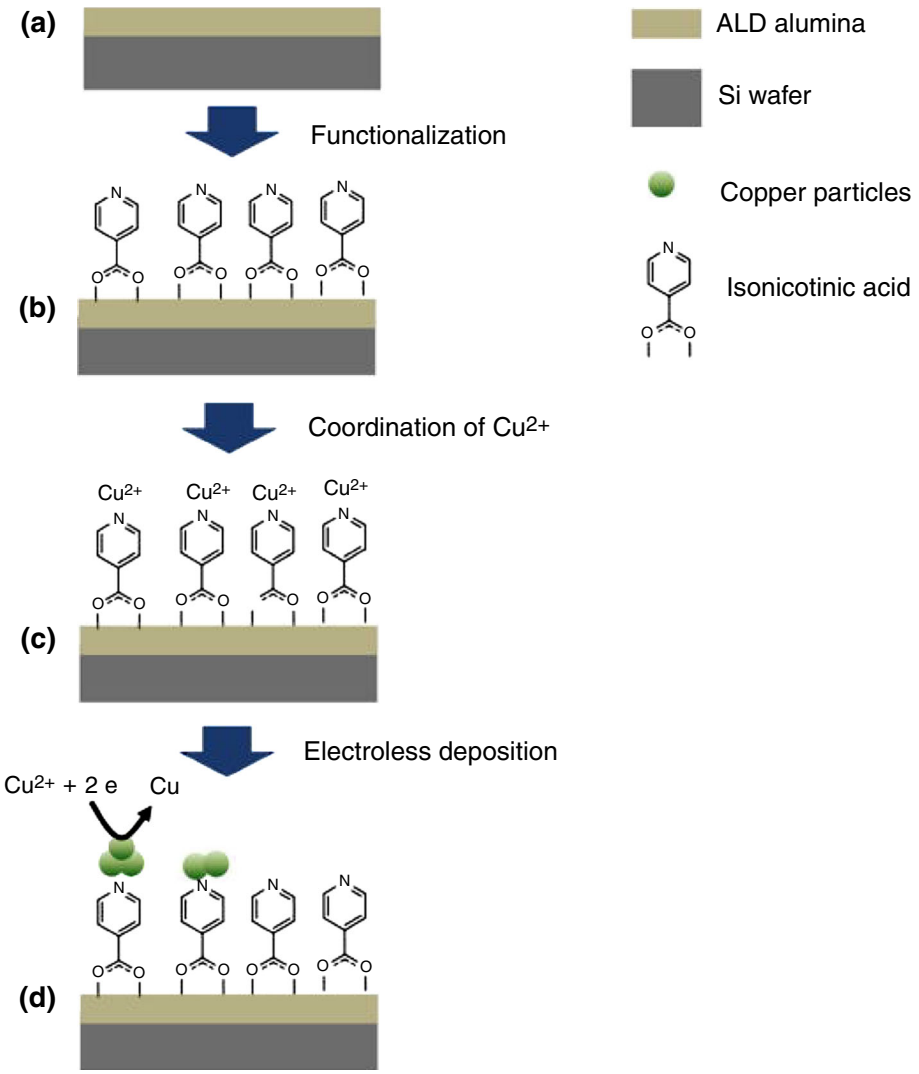

Fig. 2: Schematic illustration of the functionalization of alumina-coated Si wafer with isonicotinic acid and the subsequent electroless copper deposition reaction

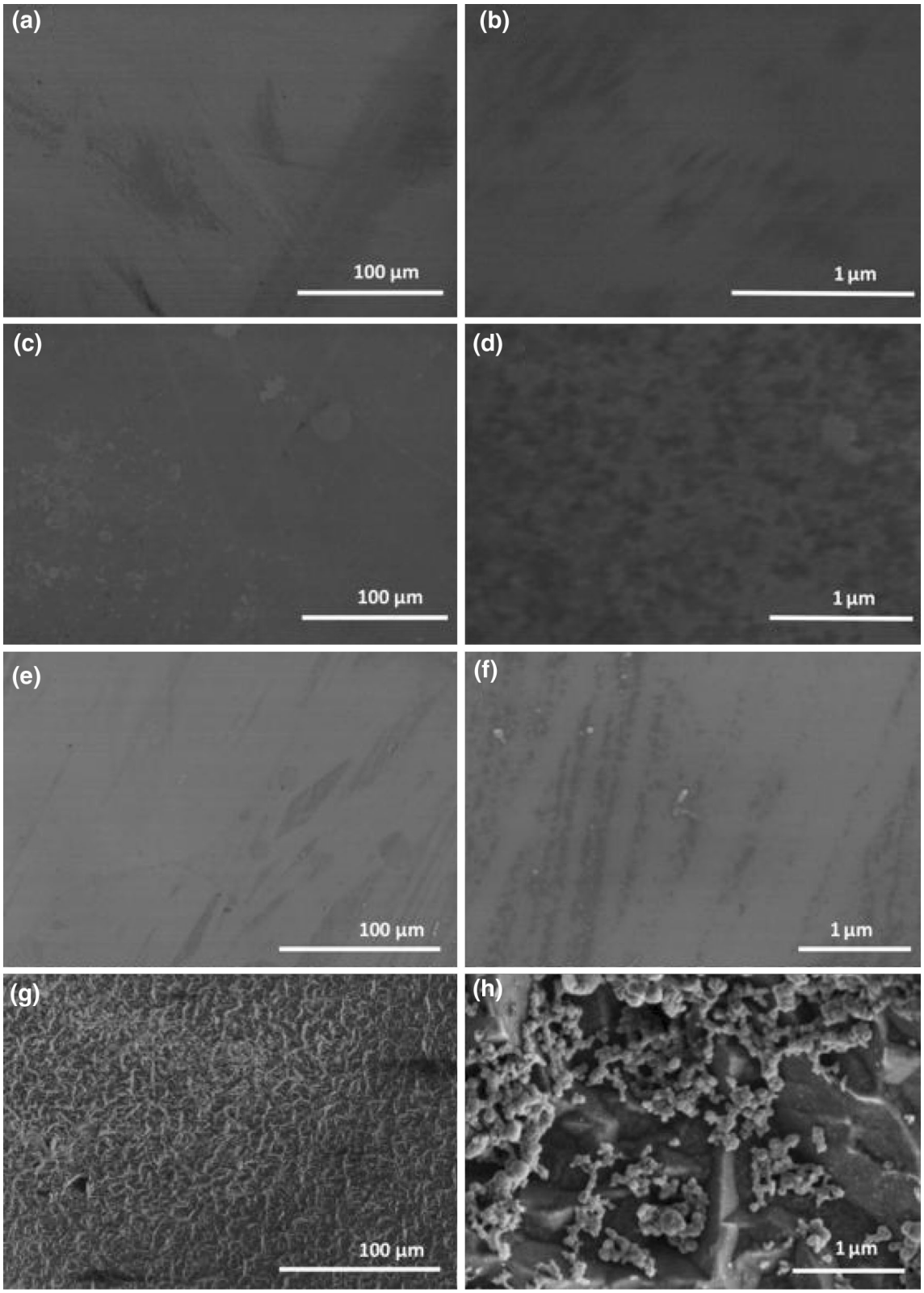

Fig. 3: SEM micrographs of untreated alumina-coated silicon wafer (a and b), *i*NA-functionalized alumina (c and d), hydrazine-activated Cu ELD on the untreated alumina (e and f), and hydrazine-activated Cu ELD on the *i*NA-functionalized alumina (g and h)

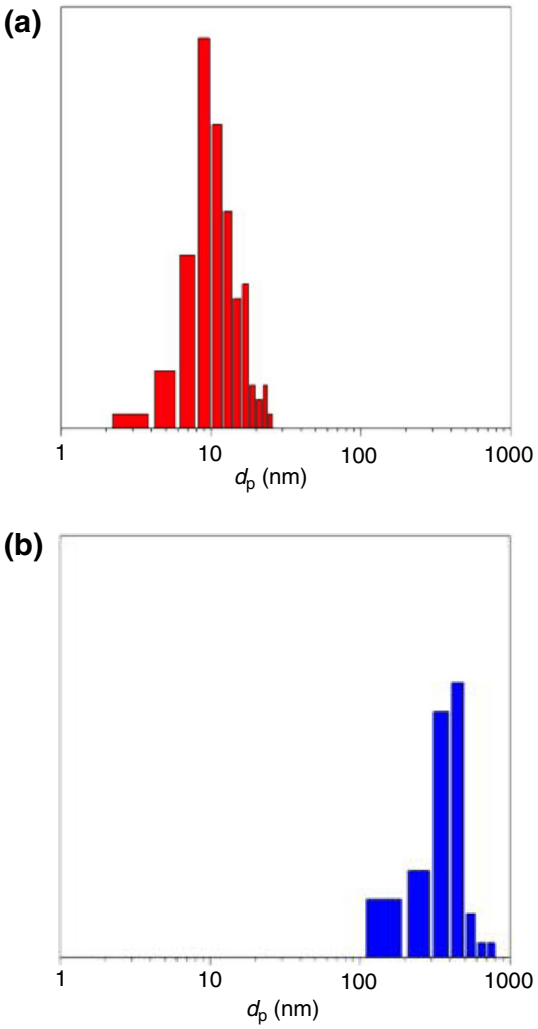

Fig. 4: Particle size distribution from SEM micrographs of Cu ELD on the *i*NA-functionalized alumina activated with (a) hydrazine and (b) formaldehyde

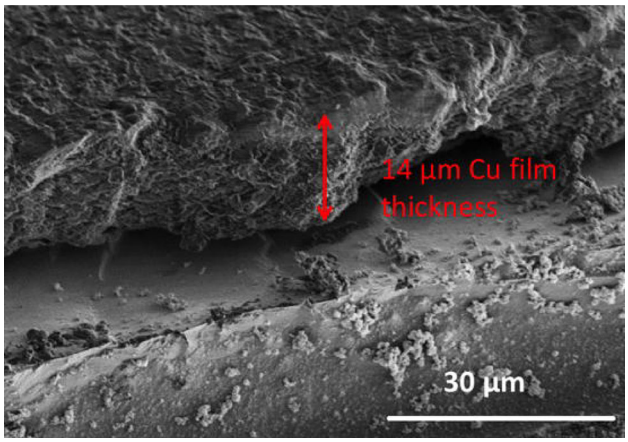

Fig. 5: SEM image of the cross section of the hydrazine-activated Cu ELD on the *i*NA-functionalized alumina wafer

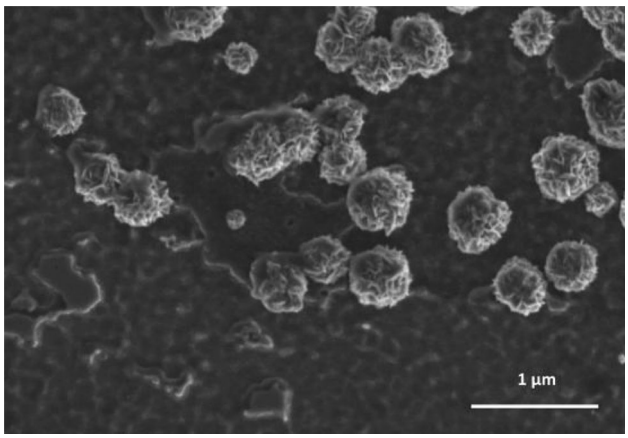

Fig. 6: SEM micrograph of formaldehyde-activated Cu ELD on the *i*NA-functionalized alumina

alization, and after electroless deposition. Typical SEM micrographs (Figs. 3a and 3b) of the alumina-coated wafer (A) before functionalization show that the surface is relatively smooth. Figures 3c and 3d show that after functionalization with isonicotinic acid (*i*NA-A) this smoothness is retained. The slight change in texturing at higher magnification (Fig. 3d as compared to Fig. 3b) is typical of the SAM formation on atomic layer-deposited alumina,[27] as a result of the solubilization (through NP formation) of some of the alumina.[24] In the absence of *i*NA functionalization, the hydrazine-activated ELD results in a surface (Figs. 3e and 3f) that is similar to the untreated sample. However, there are some discernable features that are consistent with the presence of homogeneous nucleation (see below). In contrast, after ELD and washing, the isonicotinic acid-functionalized wafer (Cu-*i*NA-A) surface consisted of a highly textured uniform coating (Fig. 3g). The surface appears to be formed from interlocking crystalline facets, which is confirmed by AFM and XRD (see below). At higher magnification (Fig. 3h), it may be seen that the faceted surface is sparsely covered in small nodular growth. The size distribution of these particles (12 ± 4 nm) is shown in Fig. 4a. A cross-sectional SEM image (Fig. 5) shows a uniform Cu layer with uniform texture throughout the film.

The use of formaldehyde as the reducing agent results in a different texture to the Cu surface (Fig. 6). The major portion of the surface appears to be far less faceted than that with the hydrazine activation. As with the hydrazine-activated ELD, there are also nodular growths on the wafer surface (Fig. 6), but these are significantly larger (150 ± 30 nm, see Fig. 4 b) and appear to grow out of the surface rather than be deposited from the solution.

AFM characterization of the different surfaces of the samples is shown in Fig. 7 and Table 1. Height measurements of the alumina-coated silicon wafer (A) revealed a relatively flat surface of around 0.1–2.0 nm

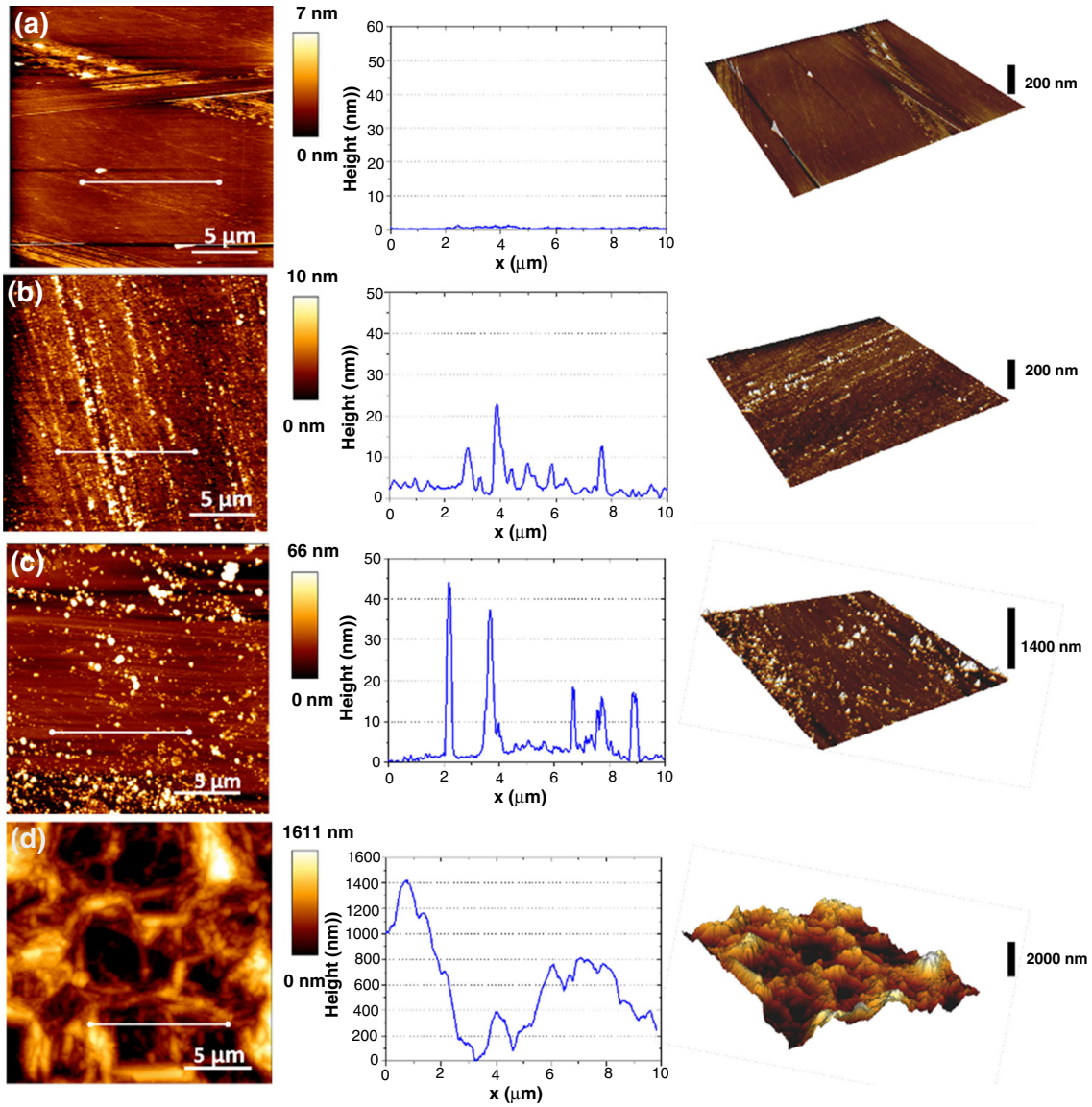

Fig. 7: AFM images, height profiles along the white line, and 3D projections of (a) alumina-coated silicon wafer (A), (b) isonicotinic acid-functionalized alumina (*i*NA-A), (c) hydrazine-activated ELD Cu on the unfunctionalized wafer (Cu-A), and (d) hydrazine-activated ELD Cu on the isonicotinic acid-functionalized alumina (Cu-*i*NA-A). Images were obtained with a scan size of 20 × 20 μm

Table 1: Values of the average roughness (R_a), mean roughness root-mean-square (R_q), and the peak-to-valley roughness (R_t) determined from the AFM scans

Sample	R_a (nm)	R_q (nm)	R_t (nm)
A	1.0 ± 0.6	3 ± 3	130 ± 90
Cu-A	8.9 ± 0.9	15 ± 2	280 ± 65
*i*NA-A	1.4 ± 0.1	2.8 ± 0.5	130 ± 10
Cu-*i*NA-A	360 ± 57	460 ± 87	3000 ± 1500

(Fig. 7a), which upon functionalization by isonicotinic acid becomes slightly rougher, i.e., 0.2–20 nm (Fig. 7b), but shows a similar R_q value to that of the unfunctionalized sample (Table 1). The AFM image of the hydrazine-activated Cu ELD on the unfunctionalized alumina surface (Fig. 7c) is consistent with the presence of 10–40 nm particles sparsely distributed on the surface. These are the same range as observed

scattered on the surface of Cu-*i*NA-A samples by SEM (Fig. 3h). However, these features are not observed in the AFM of the Cu-*i*NA-A samples (Fig. 7d) due to any such variation being swamped by the textured base layer of Cu, as seen in the associated SEM.

The formation of the textured contiguous coating (irrespective of the reducing agent) can be rationalized by assuming that the N functionalization of *i*NA–SAMs forms complexes with Cu^{2+} from solution, a heterogenous nucleation reaction continuously takes place at the surface, and the as-formed nanocrystals are assembled to a contiguous film. Support for this proposal is the observation[22] that *i*NA-functionalized alumina nanoparticle (*i*NA-NP) complex with copper acetate (CuA) to form a stable conjugate (CuA-*i*NA-NP). Thus, the *i*NA successfully directs Cu growth to the surface. The similarity in size of the particulate features in the hydrazine-activated Cu-*i*NA-A (Figs. 3h and 4a) to those in the Cu-A (Fig. 7c) suggests that these features in the Cu-A are dropped onto the surface from solution (possibly during removal of the sample from the reaction bath), rather than grown from the surface, and were subsequently not removed in the washing step.

Surface chemical composition

As expected from the ca. 1 μm^3 analysis volume of EDX, the spectra for the untreated and iNA-functionalized samples show predominantly the Si wafer substrate (Table 2) since the ALD alumina layer is ca. 500 nm. EDX analysis of the hydrazine-activated Cu ELD on the *i*NA-functionalized alumina surface (Cu-*i*NA-A) shows the expected Cu and a decrease in both Si and Al as compared to the pre-ELD substrate (*i*NA-A), see Table 2. In contrast, analysis after Cu ELD on the unfunctionalized alumina surface shows only a trace of Cu consistent with the SEM and AFM results.

Further evidence for the Cu deposition on the isonicotinic acid-functionalized alumina films was obtained from XPS (Table 3). As expected, there is a decrease in Si, Al, and O content with the formation of the Cu ELD on *i*NA-A. This is consistent with the SEM and AFM data. It is interesting to note that the N content increases after Cu deposition, although it would be expected to decrease given that the isonicotinic should be coated by the Cu (i.e., Fig. 2). However, we note that the sample prepared by Cu ELD on the unfunctionalized surface also contains nitrogen. The high-resolution N 1s peak for Cu-A and Cu-*i*NA-A is shown in Fig. 8. The presence of N in the former is presumably a residue (or a side product) from the hydrazine reducing agent,[30] which gives an almost identical binding energy to N in pyridine derivatives.[31–34] Figure 8b shows the high-resolution Cu 2p envelope where two photoelectron peaks (Cu $2p_{3/2}$ and Cu $2p_{1/2}$) can be observed for both Cu-A and Cu-*i*NA-A samples. The presence of satellite features (designated by arrows) is usually related with the presence of Cu(II) oxide.[35]

Surface and structural properties

The XRD patterns of the copper-plated pristine alumina (Cu-A) and the copper-plated isonicotinic acid-functionalized alumina (Cu-*i*NA-A) are shown in Fig. 9. The wafers comprise a ca. 500 nm layer of alumina formed on the silicon wafer by ALD, and as such, the XRD pattern is dominated by the pattern for [004] peak of the silicon wafer. As orientated Si wafers were used for all samples, in some cases peaks for the forbidden reflection [002] ($2\theta = 32.8°$) and other signals such as $2\theta = 61.7°$ and $2\theta = 65.9°$ caused either by instrumental artifacts[36] in the oriented substrate or due to the ''invisible'' laser markings on the original Si wafer are observed.[37] No peaks for the alumina are observed due to the thinness of the layer and its polycrystalline nature. However, a small peak consis-

Table 2: EDX analysis (atomic%)

Sample	Si	Al	O	C	Cu
A	71.4 ± 1.0	1.5 ± 0.1	9.4 ± 0.3	17.7 ± 1.3	0.0
Cu-A	85.0 ± 5.4	0.9 ± 0.1	5.9 ± 5.6	8.0 ± 5.3	0.2 ± 0.5
*i*NA-A	98.1 ± 1.1	0.5 ± 0.2	4.7 ± 0.7	5.6 ± 0.9	0.0
Cu-*i*NA-A	80.6 ± 12.5	0.1 ± 0.1	1.7 ± 1.0	17.9 ± 13.0	0.5 ± 0.5

Table 3: XPS analysis (atomic%)

Sample	Si 2p	Al 2p	O 1s	C 1s	N 1s	Cu 2p
A	2.03	17.70	27.4	52.85	0.0	0.0
Cu-A	14.84	7.26	16.8	58.37	1.05	1.68
*i*NA-A	4.79	19.27	44.62	30.35	0.97	0.0
Cu-*i*NA-A	11.42	9.21	21.12	52.9	2.5	2.86

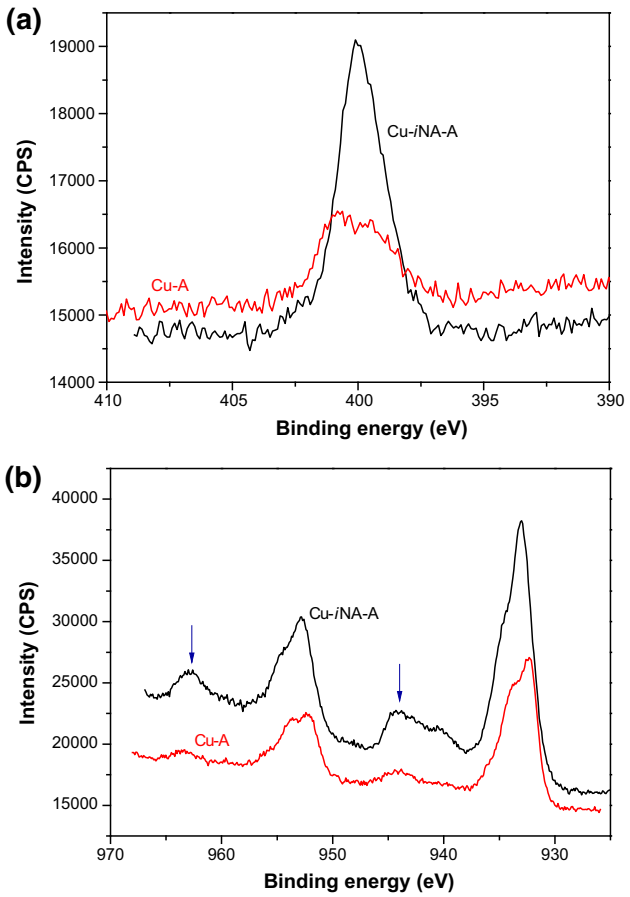

Fig. 8: High-resolution XPS spectra of (a) N 1s and (b) Cu 2p. The presence of smaller shake-up peaks in (b) is indicated

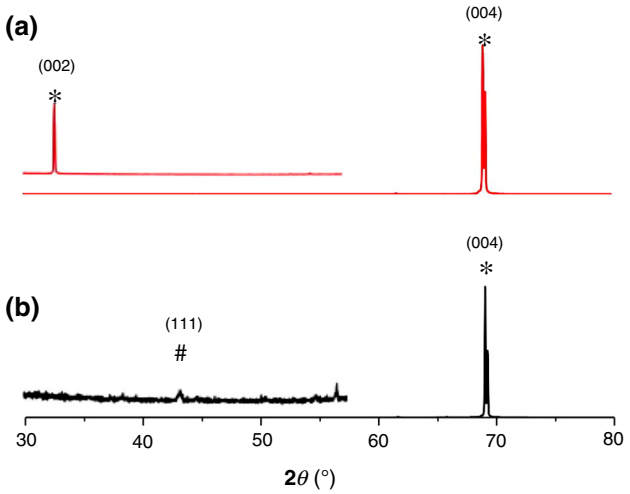

Fig. 9: XRD patterns of hydrazine-activated Cu ELD on (a) unfunctionalized alumina (A) and (b) isonicotinic acid-functionalized alumina (*i*NA-A). Si (COD 9011056)- and Cu (COD 7101264)-related signals are indicated with * and # symbols, respectively. Peaks not identified are related with the incident spectra

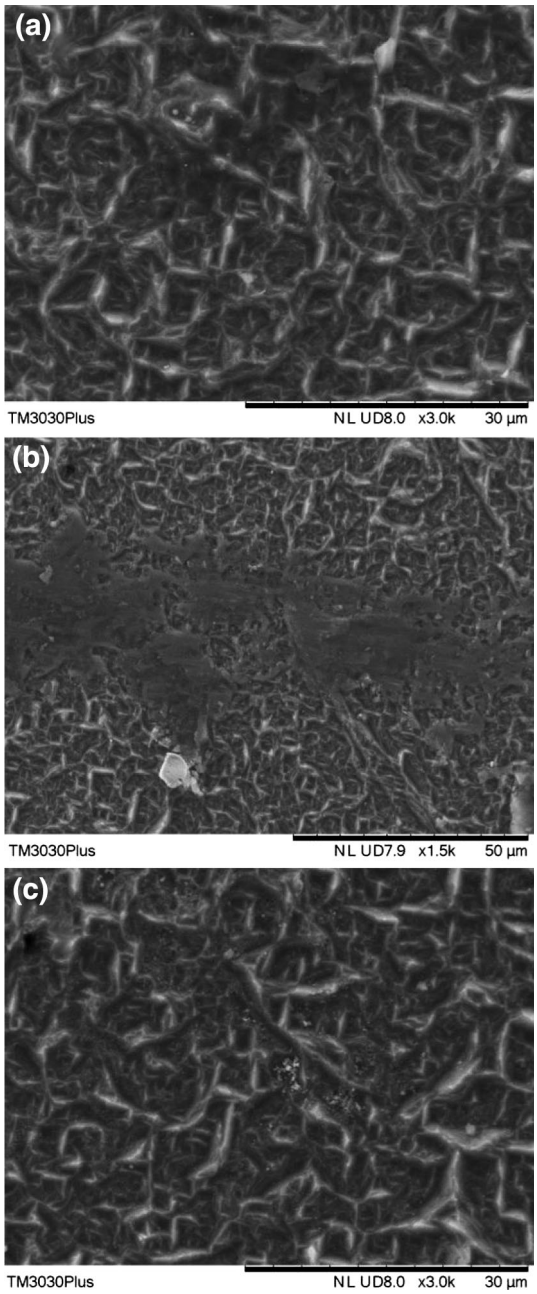

Fig. 10: SEM micrograph of (a) the surface of hydrazine-activated Cu ELD on an *i*NA-functionalized alumina wafer, (b) after being scratched with a glass cutter, and (c) after being subjected to a Scotch Tape test

tent with metallic Cu is observed ($2\theta = 43.2°$), see Fig. 9b. The confirmation of Cu^0 suggests that the Cu(II) satellites seen in the XPS are due to surface oxidation of the nanoparticles.[38]

The Cu coating was found to be highly adhesive to the substrate. An area on the surface of hydrazine-activated Cu ELD on an *i*NA-functionalized alumina wafer was scratched with a glass cutter. As can be seen

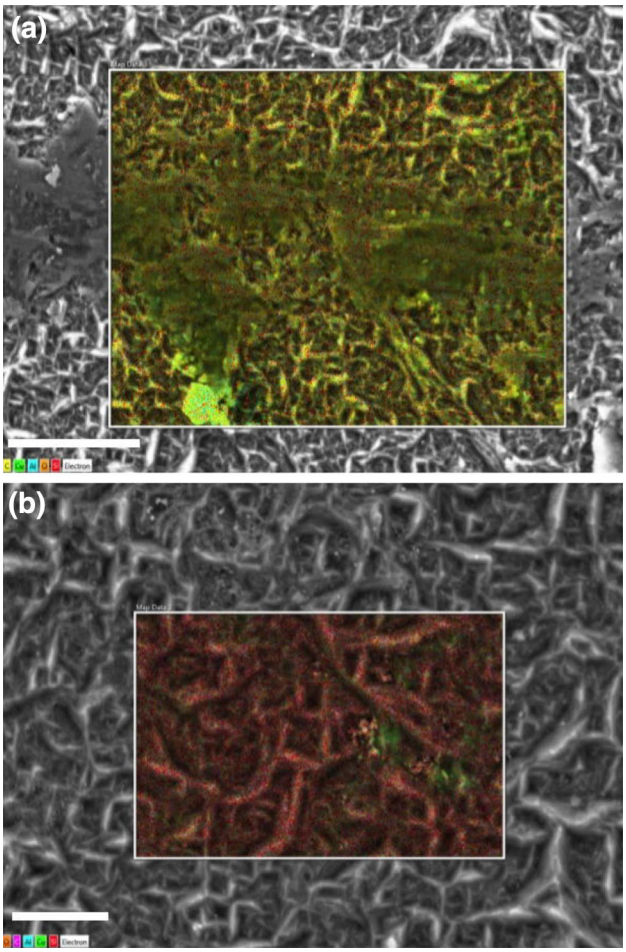

Fig. 11: Cu EDX mapping of the surface of hydrazine-activated Cu ELD on an *i*NA-functionalized alumina wafer (a) after being scratched with a glass cutter and (b) after being subjected to a Scotch Tape test. Scale bars are 25 and 10 μm, respectively

in the SEM micrographs of Figs. 10a and 10b, the scratch has changed the surface topography of the sample; however, EDX analysis of the surface after scratching (Fig. 11a) showed no variation in composition. This suggests that the surface of the Cu film is scratched as would be expected by the relative hardness of the diamond tip versus the metal, but that the film was not removed from the surface. In addition, a different area was subjected to a Scotch Tape test to probe the durability of the surface. As can be seen in Figs. 10c and 11b, there appears to be no effect on the adhesion of the film.

The water contact angles (CA) of the various functionalized and plated alumina wafers are shown in Table 4. The water CA of the Cu ELD on pristine alumina is not significantly different from the pristine alumina, while the isonicotinic acid-functionalized wafer endows the surface with a slightly higher hydrophilicity. This is consistent with previous dual functionality on alumina surfaces.[27,28] On plating with copper, this surface is rendered more hydrophobic consistent with being coated by a metallic layer.[39]

Table 4: Advancing contact angle (°)

Sample	Contact angle (°)
A	96 ± 2
Cu-A	94 ± 3
*i*NA-A	80 ± 2
Cu-*i*NA-A	119.9 ± 0.8

Conclusions

In summary, the use of an isonicotinate self-assembled monolayer (SAM) is effective at promoting the heterogenous nucleation of Cu^0 films on the surface. The high stability of the isonicotinate's pyridine Lewis base interaction with Cu^{2+} ensures the coordination.[22] Based on analogy with other Cu^{2+} complexes with pyridine-type ligands,[40,41] immobilization with isonicotinic acid ligands will reduce the reduction potential resulting in the preferential reduction of the surface-bound Cu^{2+} to Cu^0. This already-deposited copper can then act as a catalyst for the deposition of further Cu^{2+} ions from the solution, allowing the deposition to proceed in an autocatalytic manner.

Acknowledgments The authors gratefully acknowledge the financial support provided by the Sêr Cymru National Research Network in Advanced Engineering and Materials, the Office of Naval Research (N00014-15-2717), and the Robert A. Welch Foundation (C-0002). ARB acknowledges the financial support provided by the Welsh Government Sêr Cymru Chair Programme.

References

1. Osaka, T, Takano, N, "Microfabrication of Electro- and Electroless-Deposition and Its Application in the Electronic Field." *Surf. Coat. Technol.*, **169–170** 1–7 (2003)
2. Osaka, T, "Creation of Highly Functional Thin Films using Electrochemical Nanotechnology." *Chem. Rec.*, **4** 346–362 (2004)
3. Jankiewicz, BJ, Jamiola, D, Choma, J, Jaroniec, M, "Silica-Metal Core-Shell Nanostructures." *Adv. Colloid Interfac.*, **170** 28–47 (2012)

4. Subramaniam, C, Yamada, T, Kobashi, K, Sekiguchi, A, Futaba, DN, Yumura, M, Hata, K, ''One Hundred Fold Increase in Current Carrying Capacity in a Carbon Nanotube–Copper Composite.'' *Nature Comm.*, **4** 2202 (2013)
5. Koo, HC, Saha, R, Kohl, PA, ''Copper Electroless Bonding of Dome-Shaped Pillars for Chip-to-Package Interconnect.'' *J. Electrochem. Soc.*, **158** D698–D703 (2011)
6. Cho, SK, Lim, T, Lee, HK, Kim, JJ, ''A Study on Seed Damage in Plating Electrolyte and Its Repairing in Cu Damascene Metallization.'' *J. Electrochem. Soc.*, **157** D187–D192 (2010)
7. Lu, Y, Meng, X, Yi, G, Jia, J, ''In Situ Growth of CuS Thin Films on Functionalized Self-Assembled Monolayers using Chemical Bath Deposition.'' *J. Colloid Interf. Sci.*, **356** 726–733 (2011)
8. Malki, M, Rozenblat-Raz, A, Duhin, A, Inberg, A, Horvitz, D, Shacham-Diamand, Y, ''Thin Electroless Co(W, P) Film Growth on Titanium-Nitride Layer Modified by Self-Assembled Monolayer.'' *Surf. Coat. Tech.*, **252** 1–7 (2014)
9. Jie, Y, Fan, H, Niskala, JR, You, W, ''Growth of Nickel Nanoparticles on an Organic Self-Assembled Monolayer Template by Means of Electroless Plating.'' *Colloid. Surface. A*, **434** 194–199 (2013)
10. Radoeva, M, Monev, M, Ivanov, IT, Georgiev, GS, Radoev, B, ''Adhesion Improvement of Electroless Copper Coatings by Polymer Additives.'' *Colloid. Surface A*, **460** 441–447 (2014)
11. Mondin, G, Wisser, FM, Leifert, A, Mohamed-Noriega, N, Grothe, J, Dörfler, S, Kaskel, S, ''Metal Deposition by Electroless Plating on Polydopamine Functionalized Micro- and Nanoparticles.'' *J. Colloid Interf. Sci.*, **411** 187–193 (2013)
12. Mondin, G, Lohe, MR, Wisser, FM, Grothe, J, Mohamed-Noriega, N, Leifert, A, Dörfler, S, Bachmatiuk, A, Rümmel, MH, Kaskel, S, ''Electroless Copper Deposition on (3-Mercaptopropyl)triethoxysilane-Coated Silica and Alumina Nanoparticles.'' *Electrochim. Acta*, **114** 521–526 (2013)
13. Tabakovic, I, Riemer, S, Sun, M, ''Self-Assembled Monolayer of 3-*N*,*N*-Dimethylaminodithiocarbamoyl-1-Propanesulfonic Acid (DPS) used in Electrodeposition of Copper.'' *J. Electrochem. Soc.*, **160** D3197–D3205 (2013)
14. Leussing, DL, Hansen, RC, ''The Copper(II)-Pyridine Complexes and their Reaction with Hydroxide Ions.'' *J. Am. Chem. Soc.*, **79** 4270–4273 (1957)
15. Haynes, JS, Rettig, SJ, Sams, JR, Trotter, J, Thompson, RC, ''Pyrazine and Pyridine Complexes of Copper(II) Trifluoromethanesulfonate. Crystal Structure of Tetrakis(pyridine) bis(trifluoromethanesulfonato-O)copper(II) and Magnetic Exchange in (Pyrazine)bis(trifluoromethanesulfonato-O)-copper(II).'' *Inorg. Chem.*, **27** 1237–1241 (1988)
16. Allan, JR, Brown, DH, Nuttall, RH, Sharp, DWA, ''Pyridine Complexes of Iron(II), Copper(II), Zinc(II), and Cadmium(II) Halides.'' *J. Chem. Soc. A*, 1031–1034 (1966)
17. Otieno, T, Hutchison, AR, Krepps, MK, Atwood, DA, ''Synthesis and Spectral and Thermal Properties of Pyrazine-Bridged Coordination Polymers of Copper(II) Nitrate: An Experiment for Advanced Undergraduates.'' *J. Chem. Educ.*, **79** 1355–1357 (2002)
18. Allen, JJ, Barron, AR, ''Molecular Structure of $[Cu_2(MeCN)_2(\mu\text{-tpy})_2][BPh_4]_2$: A Helical Di-Cuprous Terpyridine Complex.'' *J. Chem. Crystallogr.*, **38** 879–882 (2008)
19. Allen, JJ, Barron, AR, ''Unusual Co-Crystallization of Both Monomeric and Dimeric Forms of $Cu[PhN(py)(quin)]Cl_2$.'' *J. Chem. Crystallogr.*, **41** 654–663 (2011)
20. Allen, JJ, Hamilton, CE, Barron, AR, ''Molecular Structures of RN(H)Py (R = 2,4,6-$Me_3C_6H_2$, 2,6-$Et_2C_6H_3$, Ph_3C) and the Copper Complex $[Cu\{(2,4,6\text{-}Me_3C_6H_2)N(H)Py\}_2]BF_4$.'' *J. Chem. Cryst.*, **39** 573–580 (2009)
21. Allen, JJ, Hamilton, CE, Barron, AR, ''Synthesis and Structural Characterization of $(2,6\text{-}^iPr_2C_6H_3)N(quin)_2$ and $[Cu\{(2,6\text{-}^iPr_2C_6H_3)N(quin)_2\}_2]BF_4$.'' *J. Chem. Cryst.*, **2** 130–136 (2010)
22. Gowenlock, CE, McGettrick, JD, McNaughter, PD, O'Brien, P, Dunnill, CW, Barron, AR, ''Copper-Complexed Isonicotinic Acid Functionalized Aluminum Oxide Nanoparticles.'' *Main Group Chem.*, **15** 1–15 (2016)
23. Hamilton, CE, Ogrin, D, McJilton, L, Moore, VC, Anderson, R, Smalley, RE, Barron, AR, ''Functionalization of SWNTs to Facilitate the Coordination of Metal Ions, Compounds and Clusters.'' *Dalton Trans.*, **37** 2937–2944 (2008)
24. Landry, CC, Pappè, N, Mason, MR, Apblett, AW, Tyler, AN, MacInnes, AN, Barron, AR, ''From Minerals to Materials: Synthesis of Alumoxanes from the Reaction of Boehmite with Carboxylic Acids.'' *J. Mater. Chem.*, **5** 331–341 (1995)
25. Koide, Y, Barron, AR, ''$[Al_5(^tBu)_5(\mu_3\text{-}O)_2(\mu_3\text{-}OH)_3(\mu\text{-}OH)_2(\mu\text{-}O_2CPh)_2]$: A Model for the Interaction of Carboxylic Acids with Boehmite.'' *Organometallics*, **14** 4026–4029 (1995)
26. Bethley, CE, Aitken, CL, Koide, Y, Harlan, CJ, Bott, SG, Barron, AR, ''Structural Characterization of Dialkylaluminum Carboxylates: Models for Carboxylate Alumoxanes.'' *Organometallics*, **16** 329–341 (1997)
27. Alexander, S, Morrow, L, Lord, AM, Dunnill, CW, Barron, AR, ''pH-Responsive Octylamine Coupling Modification of Carboxylated Aluminium Oxide surfaces.'' *J. Mater. Chem. A*, **3** 10052–10059 (2015)
28. Vogelson, CT, Keys, A, Edwards, CL, Barron, AR, ''Molecular Coupling Layers Formed by Reactions of Epoxy Resins with Self-Assembled Carboxylate Monolayers Grown on the Native Oxide of Aluminum.'' *J. Mater. Chem.*, **13** 291–296 (2003)
29. Ogura, T, Malcomson, M, Fernando, Q, ''Mechanism of Copper Deposition in Electroless Plating.'' *Langmuir*, **6** 1709–1710 (1990)
30. Biner, H, Sellman, DZ, ''X-ray Photoelectron Studies of Pentacarbonyl Chromium and Tungsten Complexes with Nitrogen Ligands.'' *Naturforsch*, **33b** 173–179 (1978)
31. Barber, M, Connor, JA, Guest, MF, Hillier, IH, Schwarz, M, Stacey, M, ''Bonding in Some Donor-Acceptor Complexes Involving Boron-Trifluoride—Study by Means of ESCA and Molecular Orbital Calculations.'' *J. Chem. Soc., Faraday Trans. II*, **69** 551–558 (1973)
32. Lindberg, BJ, Hedman, J, ''Molecular Spectroscopy by Means of ESCA 6 Group Shifts for N, P and As Compounds.'' *Chem. Scr.*, **7** 155–166 (1975)
33. Camalli, M, Caruso, F, Mattogno, G, Rivarola, E, ''Adducts of Tin(IV) and Organotin(IV) Derivatives with 2,2′-Azopyridine. 2. Crystal and Molecular Structure of SnMe2Br2AZP and Further Mossbauer and Photoelectronic Spectroscopic Studies.'' *Inorg. Chim. Acta*, **170** 225–231 (1990)
34. Yoshida, T, ''An X-ray Photoelectron Spectroscopic Study of Several Ligands in Coordination Compounds.'' *Bull. Chem. Soc. Jpn.*, **53** 1327–1330 (1980)
35. Kawai, J, Tsuboyama, S, Ishizu, K, Miyamura, K, Saburi, M, ''Ligand Determination of a Copper Complex by Cu 2P X-ray Photoelectron Spectroscopy.'' *Anal. Sci.*, **10** 853–857 (1994)
36. Zaumseil, P, ''High-Resolution Characterization of the Forbidden Si 200 and Si 222 Reflections.'' *J. Appl. Crystallogr.*, **48** (2) 528–532 (2015)
37. Lam, YC, Zheng, HY, Tjeung, RT, Chen, X, ''Seeing the Invisible Laser Markings.'' *J. Phys. D: Appl. Phys.*, **42** 042004 (2009)

38. Brege, JJ, Hamilton, CE, Crouse, CA, Barron, AR, ''Ultra-Small Copper Nanoparticles from a Hydrophobically Immobilized Surfactant Template.'' *Nano Lett.*, **9** 2239–2242 (2009)
39. Tao, YT, ''Structural Comparison of Self-Assembled Monolayers of n-Alkanoic Acids on the Surfaces of Silver, Copper, and Aluminum.'' *J. Am. Chem. Soc.*, **115** 4350–4358 (1993)
40. Lincoln, KM, Offutt, ME, Hayden, TD, Saunders, RE, Green, KN, ''Structural, Spectral, and Electrochemical Properties of Nickel(II), Copper(II), and Zinc(II) Complexes Containing 12-Membered Pyridine- and Pyridol-Based Tetra-aza Macrocycles.'' *Inorg. Chem.*, **53** 1406–1416 (2014)
41. Rawat, SP, Choudhary, M, ''Synthesis, Spectroscopic, and Electrochemical Studies on Some New Copper(II) Complexes Containing 2-[(Z)-Phenyl (Pyridine-2-yl) Methylidene] AminoBenzenethiol and Monodentate Ligands.'' *Int. J. Inorg. Chem.*, **2014** 618943 (2014)